IJEIT
The International Journal of Engineering and Information Technology
journal homepage:www.ijeit.misuratau.edu.ly
MISURATA UNIVERSITY

A Quantitative Numerical Study for the Interaction of Strong Shock Waves with Heterogeneous Bubbles

Shaban A. Jolgam
Department of Mechanical Engineering, University of Zawia
Zawia, Libya

Ahmed R. Ballil
Department of Mechanical Engineering, University of Benghazi
Benghazi, Libya

Andrzej F. Nowakowski
Sheffield Fluid Mechanics Group SFMG, Department of Mechanical Engineering, University of Sheffield
Sheffield, Uk

Abdulmaged K. Shati
Department of Mechanical Engineering, University of Zawia
Zawia, Libya

Abstract— **A qualitative and quantitative numerical study of compressible flows characterized by various physical properties jumps across the interface is presented in this work. Interactions of strong planar shock waves of high Mach numbers (1.5 ≤ Ma ≤ 3) with cylindrical gas bubbles are examined under re-shock conditions. Three distinctive gas bubbles which are Helium, Nitrogen and sulfur-hexaflouride surrounded by air that produce heavy/light, close molecular weight and light/heavy configurations are considered. To capture the interface evolution in two-component flows a diffuse interface technique is utilized. A numerical algorithm is constructed to solve the reduced hyperbolic six-equation model with a single velocity and two pressures. The approximate HLL Riemann solver scheme is used with an extended second order finite volume Godunov type approach. The non-conservative equations and terms which are essential part of the model to accomplish the interface conditions are considered by the implemented numerical scheme. The computed results using a moderate shock velocity (Ma = 1.5) moving through an open shock tube are compared with published experimental data. The computations are extended to consider both high Mach numbers and re-shock conditions. The physical behavior of these various flow systems is reproduced by the obtained results. All investigated cases show the effect of molecular weight, density and Mach number on the interface evolution and the vortex formation.**

Index Terms: **compressible two-component flow, six-equation model, HLL Riemann solver, density ratio, interface evolution, Richtmyer-Meshkov instability, shock-bubble interaction.**

I. INTRODUCTION

Compressible two-component flows characterized by low to high molecular weight ratios between the constituents are common in many industrial and engineering applications such as oil and gas industry, fuel injection and atomization systems. A well known physical phenomenon in this field is the Richtmyer-Meshkov Instabilities (RMI). This hydrodynamic instability of the interfaces between flow components appears when a shock wave accelerates inhomogeneous flows. A typical problem for studying the interface perturbation and deformation is the interaction of a planar shock wave with a single spherical or cylindrical bubble. The propagation of a shock wave through inhomogeneous media gives increase to distinctive fluid motions that affect the characteristics of the flow such as, the formation of vortices and turbulence generation and mixing. A good example of this phenomenon is the supersonic combustion in aircraft engines [1] and the inertial confinement fusion (ICF) [2].

Many experiments have been carried out to investigate the nature and the details of the interface instability resulting from the shock-bubble interaction. The first group of shock–bubble interaction experiments have been performed with shadowgraph diagnostic techniques, starting from the innovative work of [3] to the series of experiments of [4-6]. The second group of the RMI and shock–bubble interaction experiments have been conducted using modern Laser technologies, see for example [7,8]. All these significant experiments allow us to better understand the mechanism of the shock-bubble interaction and provide precise details about the related physical phenomena such as the generation of RMI. A valuable review article on advances in experimental studies of the instability of interfaces induced by shock waves has been written by [9].

Further to these experimental studies, many numerical studies have been made to reproduce interface evolution and RMI induced by shock-bubble interaction and to investigate and describe the physics of these phenomena, see for example [5,10-13]. In the latter references, some quantitative comparisons between experimental and numerical results for shock-bubble interactions are provided. Further computational studies for the shock

Received 19Oct ,2020; revised 10 Nov, 2020; accepted 17 Nov, 2020.

Available online 29 Nov, 2020.

bubble interaction that consider the effect of various flow parameters on the interface perturbation and evolution are available in literature e.g. [14-16]. A clear description of various physical phenomena associated with shock-bubble interaction has been presented in [17].

The investigation of shock-bubble interactions and RMI has been extended to study the interactions with re-shock conditions. In this framework; an experimental study of the interaction of a planar shock wave with a spherical bubble under re-shock was presented in [18]. The effect of incident shock wave strength on the decay of interface-induced perturbations in the refracted shock wave was studied numerically in [19]. The creation and the evolution of the vortex rings induced by interactions between shock waves and a low-density bubble were studied in [20].

In this contribution further investigations of the deformation and instability of different density cylindrical bubbles induced by an incident shock and its reflected shock waves are presented by using the diffuse interface simulation method. The computational model is firstly validated by experimental results from the literature and is further used to study the effect of incident shock wave strength on the interface evolution and the generation of the vorticity field.

This paper consists of five sections. In section 2, the governing equations are reviewed. Then in section 3, the numerical method is briefly explained. Summary of obtainedresults together with their discussion are presented in section 4. This is finally followed by conclusions.

II. THE GOVERNING EQUATIONS

The considered two-component flow model was formerly derived in [21]. In two-dimensional space, the model consists of seven equations. It is structured as: two continuity equations, a mixture momentum equation in x-direction, a mixture momentum equation in y-direction, two internal energy equations and a volume fraction equation. This model has been chosen for numerical simulations because it has a number of significant mathematical and numerical advantages with respect to the pressure equilibrium condition, for more details see [22].

For compressible flows without mass and heat transfer the model can be written as follows:

$$
\begin{aligned}
&\frac{\partial \alpha_1}{\partial t} + u\frac{\partial \alpha_1}{\partial x} + v\frac{\partial \alpha_1}{\partial y} = \mu(p_1 - p_2),\\
&\frac{\partial \alpha_1\rho_1}{\partial t} + \frac{\partial \alpha_1\rho_1 u}{\partial x} + \frac{\partial \alpha_1\rho_1 v}{\partial y} = 0,\\
&\frac{\partial \alpha_2\rho_2}{\partial t} + \frac{\partial \alpha_2\rho_2 u}{\partial x} + \frac{\partial \alpha_2\rho_2 v}{\partial y} = 0,\\
&\frac{\partial \rho u}{\partial t} + \frac{\partial(\rho u^2 + (\alpha_1 p_1 + \alpha_2 p_2))}{\partial x} + \frac{\partial \rho uv}{\partial y} = 0,\\
&\frac{\partial \rho v}{\partial t} + \frac{\partial \rho uv}{\partial x} + \frac{\partial(\rho v^2 + (\alpha_1 p_1 + \alpha_2 p_2))}{\partial y} = 0,\\
&\frac{\partial \alpha_1\rho_1 e_1}{\partial t} + \frac{\partial \alpha_1\rho_1 e_1 u}{\partial x} + \frac{\partial \alpha_1\rho_1 e_1 v}{\partial y}\\
&+ \alpha_1 p_1\frac{\partial u}{\partial x} + \alpha_1 p_1\frac{\partial v}{\partial y} = -p_i\mu(p_1 - p_2),\\
&\frac{\partial \alpha_2\rho_2 e_2}{\partial t} + \frac{\partial \alpha_2\rho_2 e_2 u}{\partial x} + \frac{\partial \alpha_2\rho_2 e_2 v}{\partial y}\\
&+ \alpha_2 p_2\frac{\partial u}{\partial x} + \alpha_2 p_2\frac{\partial v}{\partial y} = p_i\mu(p_1 - p_2).
\end{aligned}
\tag{1}
$$

where α_k, ρ_k, p_k, e_k are the volume fraction, density, pressure and internal energy of the component k (1 or 2), p_i is the interfacial pressure, ρ is the mixture density, u is mixture velocity in x direction, v is mixture velocity in y direction and μ is a positive constant.

In addition to the system of equations (1), an additional equation has been derived and considered in the numerical solution of the model (equation 2). This additional equation represents the mixture energy equation, which is essential for the numerical solution of the internal energy equations of the constituents. The role of the mixture equation is to correct the errors from numerical approximations of the two non-conservative constituent internal energy equations in the presence of shocks [22].

$$
\begin{aligned}
&\frac{\partial \rho E}{\partial t} + \frac{\partial u(\rho E + (\alpha_1 p_1 + \alpha_2 p_2))}{\partial x}\\
&+ \frac{\partial v(\rho E + (\alpha_1 p_1 + \alpha_2 p_2))}{\partial y}.
\end{aligned}
\tag{2}
$$

where the mixture total energy E is given by:

$$
E = \frac{\alpha_1\rho_1}{\rho}e_1 + \frac{\alpha_2\rho_2}{\rho}e_2 + \frac{1}{2}u^2 + \frac{1}{2}v^2 \tag{3}
$$

The stiffened gas equation of state is utilized for each component to establish the thermodynamic variables and has the following form:

$$
p_k = (\gamma_k - 1)\rho_k e_k - \gamma_k \pi_k \tag{4}
$$

where γ_k and π_k are the adiabatic gas constant and the pressure constant. The stiffened equation of state for the mixture can be written in the following compact form:

$$
p = \frac{\rho e - \sum_k^2 (\frac{\alpha_k \gamma_k \pi_k}{\gamma_k - 1})}{\sum_k^2 (\frac{\alpha_k}{\gamma_k - 1})} \tag{5}
$$

where p and e are the mixture pressure and mixture internal energy, respectively.

III. NUMERICAL SCHEME

The considered numerical method takes into account the discretization of the non-conservative equations and non-conservative terms that exist in the two-component flow model (1). The numerical method is developed based on the principle of Strang splitting method [23], where the model is divided into two parts. The first part is the hyperbolic operator and the second part is the pressure relaxation operator, which are solved in succession.

The hyperbolic part is solved using an extended finite volume Godunov approach. The classical Monotonic Upstream-centered Scheme for Conservation Laws (MUSCL) scheme is utilized to achieve second order accuracy in terms of the primitive variables.

The general two dimensional Godunov scheme can be written as follows:

$$U_{i.j}^{n+1} = U_{i,j}^{n} - \frac{\Delta t}{\Delta x}[F(U^{*}(U_{i,j}^{n}, U_{i+1,j}^{n})) - F(U^{*}(U_{i-1,j}^{n}, U_{i,j}^{n}))] - \frac{\Delta t}{\Delta y}[G(U^{*}(U_{i,j}^{n}, U_{i,j+1}^{n})) - G(U^{*}(U_{i,j-1}^{n}, U_{i,j}^{n}))]. \quad (6)$$

where n is time node and $n + 1$ is new time node, U is the conservative vector, Δt is the time step, $F(\underline{U})$ and $G(U)$ are flux functions in the x and y directions, respectively, i and j are the index for a computational cell i and j, respectively. Equation (6) is applied to the mass, momentum and total energy equations, where the flux functions are obtained using the extended HLL (Harten Lax and van Leer) approximate Riemann solver for Euler equations.

Similarly, the non-conservative equations for the volume fraction and two internal energies are discretized for a regular quadratic mesh as follows:

$$\alpha_{1i,j}^{n+1} = \alpha_{1i,j}^{n} - \frac{\Delta t}{\Delta x} u_{i,j}[(u\alpha_1)_{i+1/2,j}^{*} - (u\alpha_1)_{i-1/2,j}^{*} - \alpha_{1i,j}^{n}(u_{i+1/2,j}^{*} - u_{i-1/2,j}^{*})] - \frac{\Delta t}{\Delta y} v_{i,j}[(v\alpha_1)_{i,j+1/2}^{*} - (v\alpha_1)_{i,j-1/2}^{*} - \alpha_{1i,j}^{n}(v_{i,j+1/2}^{*} - v_{i,j-1/2}^{*})]. \quad (7)$$

and

$$(\alpha\rho e)_{ki,j}^{n+1} = (\alpha\rho e)_{ki,j}^{n} - \frac{\Delta t}{\Delta x} u_{i,j}[(\alpha\rho eu)_{ki+1/2,j}^{*} - (\alpha\rho eu)_{ki-1/2,j}^{*} - (\alpha p)_{ki,j}^{n}(u_{i+1/2,j}^{*} - u_{i-1/2,j}^{*})] - \frac{\Delta t}{\Delta y} v_{i,j}[(\alpha\rho ev)_{ki,j+1/2}^{*} - (\alpha\rho ev)_{ki,j-1/2}^{*} - (\alpha p)_{ki,j}^{n}(v_{i,j+1/2}^{*} - v_{i,j-1/2}^{*})] \quad (8)$$

For the pressure relaxation part, the system (9) is solved based on the instantaneous pressure relaxation assumption, where the variable μ in the relaxation terms is considered to be infinite. The procedure 4 of the iterative relaxation method introduced in [24] is utilized to perform the direct integration of the system (9). The computed volume fraction and the mixture energy ρe are used to obtain the mixture pressure from the mixture equation of state (5).

$$\begin{aligned}
&\frac{\partial \alpha_1}{\partial t} = \mu(p_1 - p_2),\\
&\frac{\partial \alpha_1\rho_1}{\partial t} = 0,\\
&\frac{\partial \alpha_2\rho_2}{\partial t} = 0,\\
&\frac{\partial \rho u}{\partial t} = 0,\\
&\frac{\partial \rho v}{\partial t} = 0,\\
&\frac{\partial \alpha_1\rho_1 e_1}{\partial t} = -p_i\mu(p_1 - p_2),\\
&\frac{\partial \alpha_2\rho_2 e_2}{\partial t} = p_i\mu(p_1 - p_2).,\\
&\frac{\partial \rho E}{\partial t} = 0.
\end{aligned} \quad (9)$$

IV. RESULTS AND DISCUSSION

In the first part of this section the developed algorithm is validated against experimental data from the open literature using open shock tube. Then, in the second part more computation cases are used to examine the effect of incident shock wave strength on the evolution of the interface and the generation of the vorticity field under re-shock condition (closed shock tube).

V. VALIDATION AGAINST EXPERIMENTAL DATA

Here two case studies are considered to validate the reliability of the developed numerical algorithm. These cases include the interaction of a moderate shock wave Ma = 1.5 with a helium (He) bubble and a nitrogen (N_2) bubble respectively, these cases were performed experimentally in [5,6]. The computational domain and initial data are shown in figure 1 and Table 1, respectively.

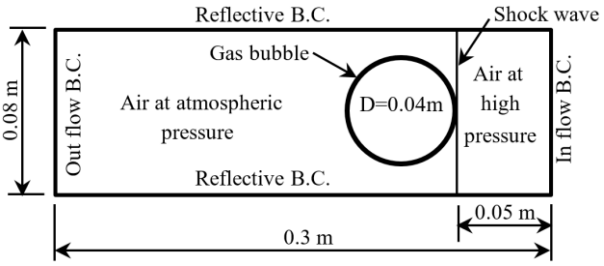

Figure 1. The Computational Domain and Initial Condition for Shock-Bubble Interaction Test Problems

Table 1. Initial conditions for validation test problems.

Physical property	Air	He	N_2	Post shock
ρ, kg/m^3	1.29	0.167	1.25	2.4021
M_w,g/mol	29	4	28	-
p, pa	101325	101325	101325	249091
u, m/s	0.0	0.0	0.0	230.28
v, m/s	0.0	0.0	0.0	0.0
γ	1.4	1.67	1.67	1.4

The numerical results show a very good agreement with the experimental data published in [5,6]. The growth of the interface with time and the shape of the contours for both gas bubbles are captured correctly (figures 2 and 3). These figures also show a set of the wave configurations that appear due to the interactions.These waves are the incident shock that propagates outside the bubble boundary, the transmitted shock wave that propagates inside the gas bubble and the reflected wave that propagates backward. The transmitted shock in the case of He bubble propagates faster than the incident wave because of the difference in acoustic impedance between the He and the surrounding air. This process together with the effect of baroclinic vorticity deposition, which is caused by the misalignment between the density and pressure gradients causes perturbation and deformation to the interface, create a kidney shape in the early stages of the interaction and is then divided into two separate contours.

In the case of the N_2 bubble the compression dominates over the interface evolution as both the molecular weight difference and interface density jump are small. Therefore, the resulting vorticity field is weak and its effect on the interface deformation can be neglected. The positions of the incident shock wave and the transmitted shock wave are illustrated in figure 4.

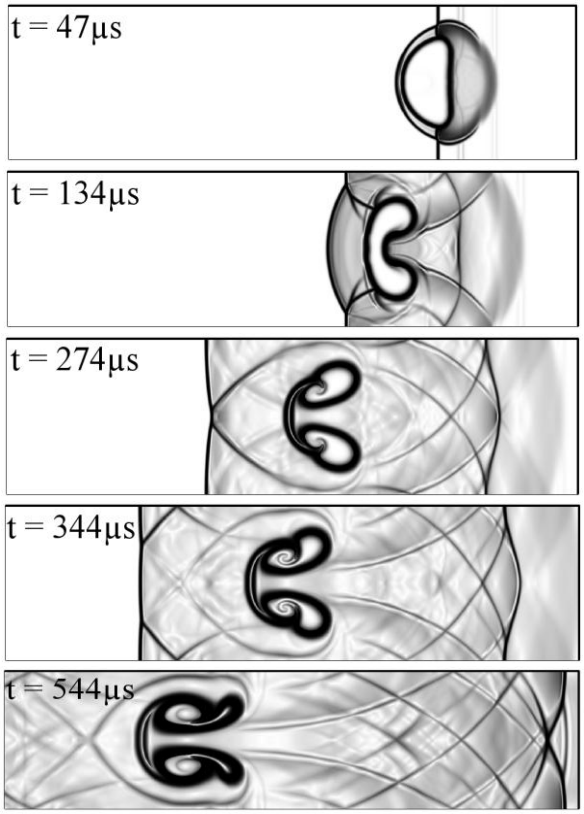

Figure 2. The Mixture Density Contours for He Bubble at Times 47, 134, 274, 344 and 544 μs for Ma =1.5.

Figure 5 shows quantitative data for the evolution of the length of the He bubble and the reduction of the N_2 bubble diameter (L/D_o) as a function of time. D_o is the initial diameter of the He and N_2 bubbles and L is a characteristic dimension of the gas bubbles for an arbitrary time as shown in figure 5a. Figures 4 and 5b could be compared with the reference experimental data and it can be concluded that the results are in a good agreement.

VI. EXTENSION OF THE NUMERICAL EXPERIMENTS

In this part the numerical experiments are extended for higher shock wave velocities and for three air/bubble configurations, which are initially at atmospheric pressure. These configurations are air/helium (He), air/nitrogen (N_2) and air/sulfur-hexaflouride (SF_6), which represent heavy/light, close molecular weight and light/heavy configuration, respectively. The bubbles are subjected to re-shock condition. The computational domain is similar to the domain in figure 1 except that the outflow boundary condition is replaced by a wall. Therefore, after the planar shock wave has interacted with a gas bubble and reached the wall it will reflect and re-interact with the bubble causing more deformation to the interface. The summary of the initial data is presented in Tables 2 and 3.

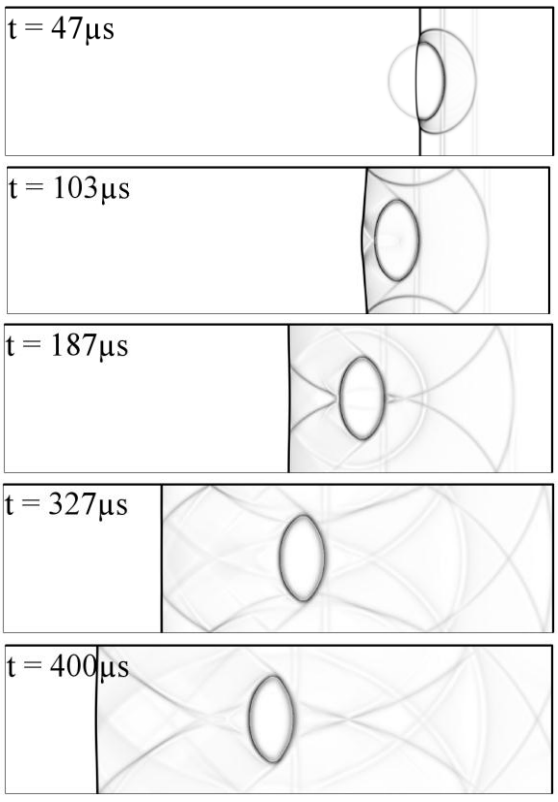

Figure 3. The Mixture Density contours for N_2 Bubble at Times 47, 103, 187, 327 and 400 μs for Ma =1.5.

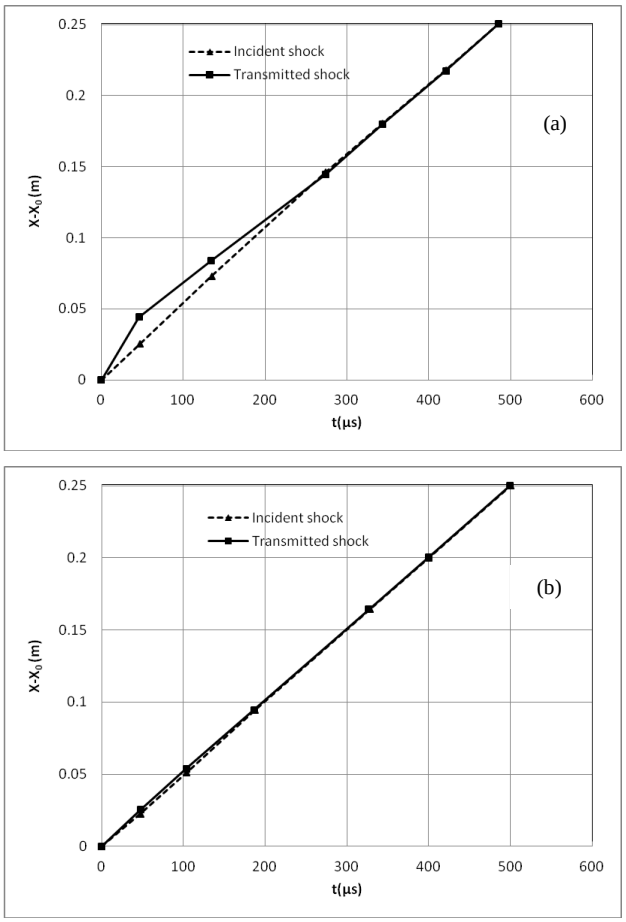

Figure 4. The recorded positions of the incident and transmitted shock waves for (a) He bubble and (b) N_2 bubble.

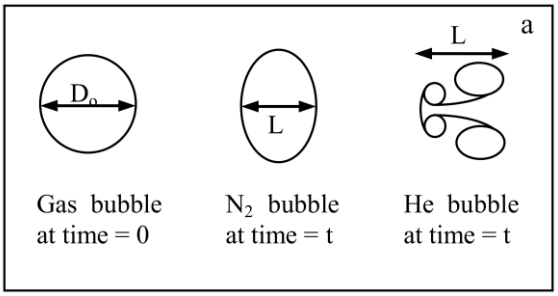

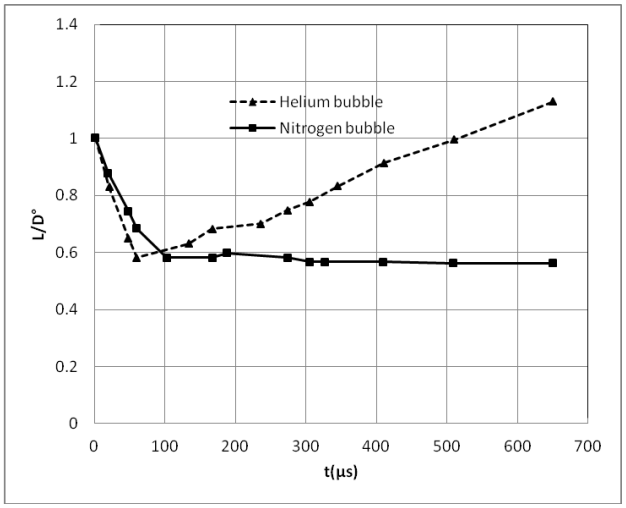

Figure 5. The evolution of the He and N_2 bubble sizes as a function of time for Ma = 1.5.

Table 2. Initial conditions for pre shock gas chamber

Physical property	Air	He	N_2	SF_6
ρ, kg/m^3	1.29	0.167	1.25	6.44
p, pa	101325	101325	101325	101325
u, m/s	0.0	0.0	0.0	0.0
v, m/s	0.0	0.0	0.0	0.0
γ	1.4	1.67	1.67	1.08

Table 3. Initial conditions for air at post shock chamber.

ρ, kg/m^3	p, pa	γ	Ma
2.4021	249091	1.4	1.5
2.8351	324747	1.4	1.7
3.8071	555261	1.4	2.2
4.9757	1047025	1.4	3.0

The different air/bubble configurations usually articulated in terms of the Atwood number (A), which is defined as $A=(\rho_1-\rho_2)/(\rho_1+\rho_2)$ where ρ_1 and ρ_2 are respectively the densities of the bubble and of the surrounding fluid. Therefore, the Atwood number A for the considered configurations has a negative value of (-0.77) in the case of He bubble, a value close to zero (-0.0157) in the case of N_2 and a positive value of 0.666 for the SF_6 bubble.

Figure 6 shows the volume fraction contours of the He bubble just before re-shock (on the left) and after the passage of the reflected wave (on the right) for different Mach numbers. One can notice that the He bubble has already separated into two entities before the re-shock process because of the interaction with the first normal shock wave and at this stage the vortical flow dominates the flow. Also it is clear that the higher Ma produces higher deformation for the bubble. After the re-shock the deformation and the growth of the bubble interface are increased in all cases. It is worth saying that as the size of the domain is fixed, the shock with the higher Ma reflects from the wall quicker. Therefore, the shock-bubble interaction for high Ma occurs in a shorter time than for low shock celerities.

Figure 7 shows the circulation Γ of the generated vortices as a function of time for several Mach numbers on the symmetric half of the domain. As we can see from this figure, the higher the Ma the higher the circulation produced, which means better mixing between working fluids. One can also notice from this figure the jump in the values of the circulation due to the effect of the interaction with the reflected wave after around 400μs for Ma = 2.2, 500μs for Ma = 1.7 and after 650μs for Ma = 1.5. Table IV shows a comparison of the values of the circulation on the symmetric half of the domain just before and after the passage of the reflected wave through the He bubble for various shock celerities.

Figure 8 presents the volume fraction contours of the N_2 bubble just before the passage of the reflected shock (on the left) and at the moment after the re-shock process (on the right) for several Mach numbers. The main physical process that dominates the interface evolution is the compression process. The higher Ma causes more compression of the N_2 bubble. This is increased after the passage of the reflected shock. Figure 9 shows a comparison of the values of the circulation as a function

of time for different Ma. Although the values of the circulation in the case of the N_2 bubble are relatively low (due to the small density jump across the interface), its value rises with the Ma number. A comparison between the values of the circulation on the symmetric half of the domain just before and after the re-shock process for different Ma is summarized in Table 5.

Table 4. Circulations (m2/s) for a He bubble subjected to shock wave accelerations of different Mach numbers.

Ma	Γ before re-shock	Γ after re-shock
1.5	15.7219	28.5135
1.7	19.5370	30.3428
2.2	28.0532	34.4857
3.0	45.5155	47.9358

Table 5. Circulations (m2/s) for a N2 bubble subjected to shock wave accelerations of different Mach numbers.

Ma	Γ before re-shock	Γ after re-shock
1.5	1.5660	1.6939
1.7	2.4932	2.8271
2.2	4.6235	5.2399
3.0	8.8657	9.2298

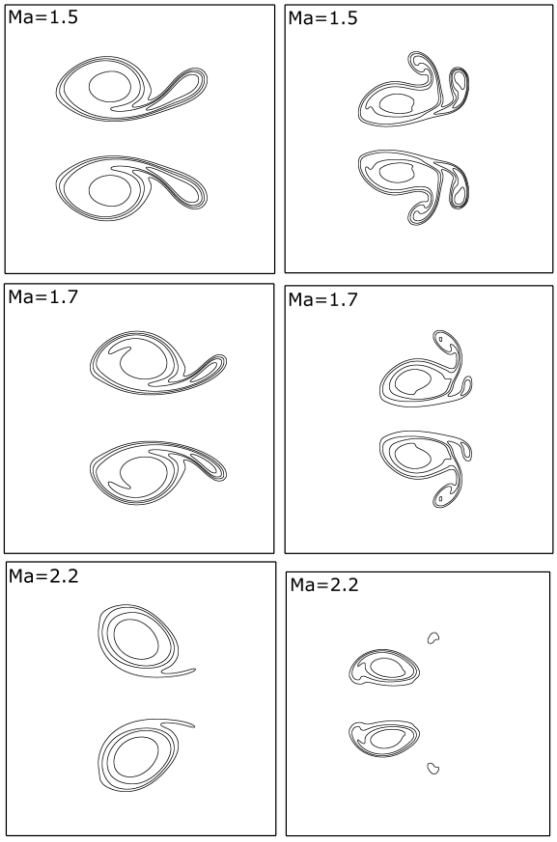

Figure 6. Volume fraction contours for He bubble at different Ma just before re-shock (left) and after re-shock (right).

Similarly, figure 10 shows the volume fraction contours of the SF_6 bubble for several Ma number cases. The contours on the left hand side represent the bubble just before the re-shock process and the contours on the right hand side represent the bubble just after the passage of the reflected shock. In contrast to the case of N_2, the growth and the evolution of the interface in this case is more visible. This is because of the larger differences in density and acoustic impedance between SF_6 and air. It is also because of the vorticity generation due to the baroclinic effect, which trigger the Richtmyer–Meshkov instability (RMI). After the passage of the reflected shock the evolution of the interface is increased in all cases. The deformation of the interface at the later stage of the interaction is governed by the vortical flow. Figure 11 shows the circulation of the symmetric half of the domain as a function of time. As in the previous cases, the higher the Ma the higher the circulation generated in the domain. Table 6 shows a comparison of the values of the circulation on the symmetric half of the domain just before and after the passage of the reflected shock through the SF_6 bubble.

From figures 6, 8 and 10, it is clear that the growth and the evolution of the interface both depend strongly on the Atwood number and molecular weight ratio. The larger *A* leads to more interface deformation than the small *A*. Also the results reveal that the larger the molecular weight ratio leads to more interface growth and deformation than the small molecular weight ratio. The vorticity effect on the interface evolution becomes more visible in the case of a large *A* and it controls the interface deformation at a later stage of the shock-bubble interaction. Also it is observable that high Ma causes more growth and perturbation to the interface than the low Ma.

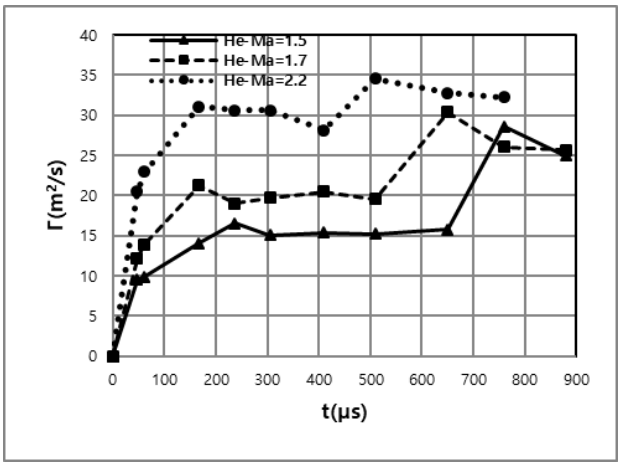

Figure 7. Circulation of a He Bubble Subjected to a Shock Wave Acceleration of Different Ma Under Re-shock Condition.

Table 6. Circulations (m2/s) for a SF6 bubble subjected to shock wave accelerations of different Mach numbers.

Ma	Γ before re-shock	Γ after re-shock
1.5	-28.1840	-30.9106
1.7	-34.9466	-40.2808
2.2	-57.1359	-67.1582
3.0	-80.0147	-87.6092

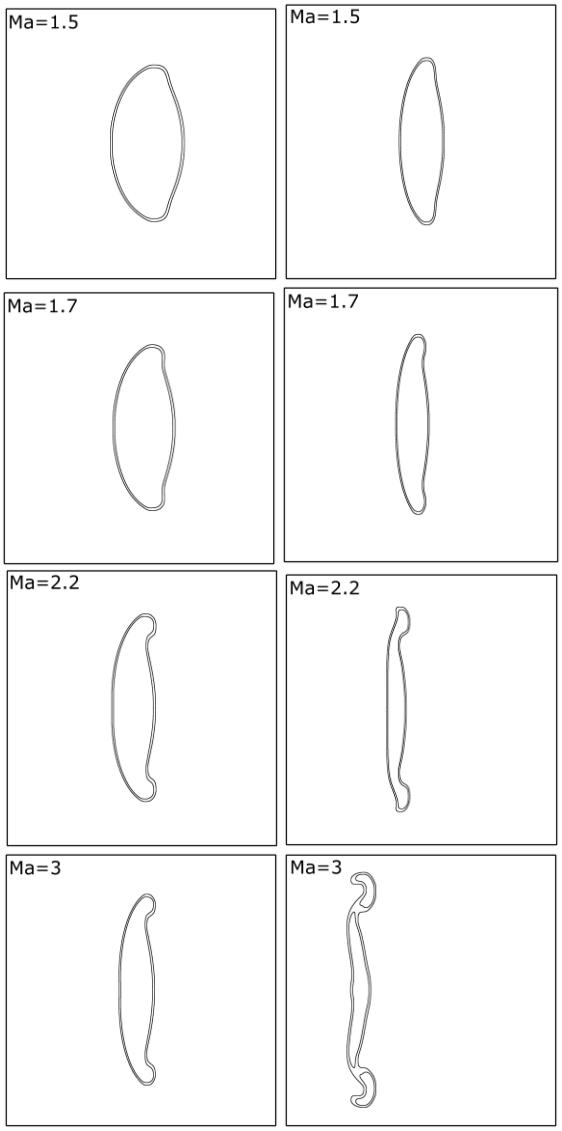

Figure 8. Volume Fraction Contours for N_2 Bubble at Different Ma Just Before re-shock (left) and after re-shock (right).

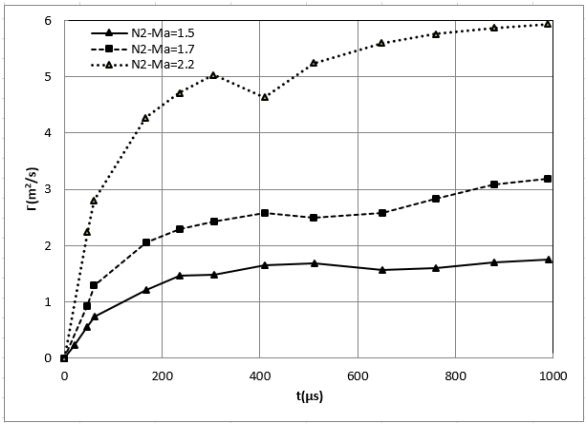

Figure 9. Circulation of a N_2 Bubble Subjected to a Shock Wave Acceleration of Different Ma Under Re-shock Condition.

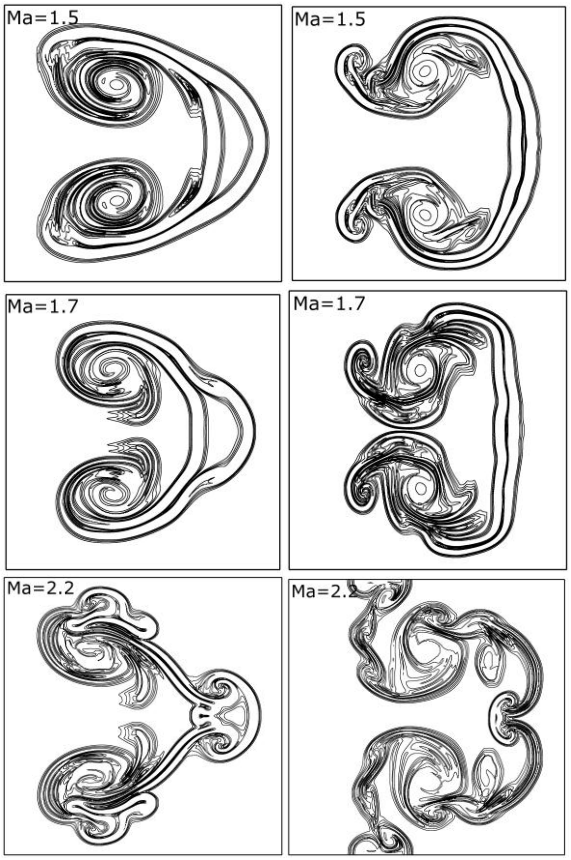

Figure 10. Volume Fraction Contours for SF_6 Bubble at Several Ma Just Before Re-shock (left) and After Re-shock (Right).

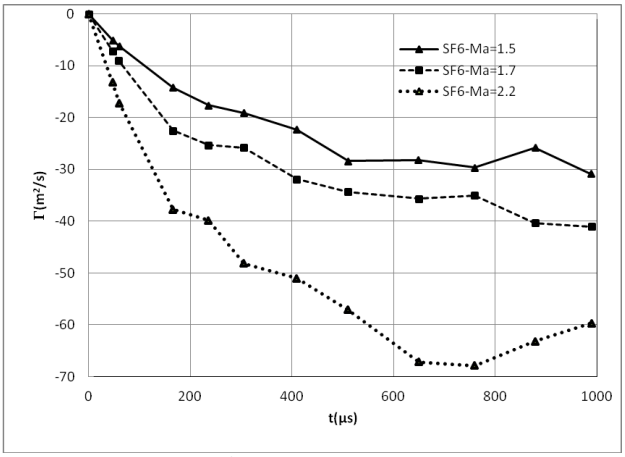

Figure 11. Circulation of a SF_6 Bubble Subjected to a Shock Wave Acceleration of Different Ma under re-Shock Condition.

From figures 7, 9 and 11 and from Tables 4, 5 and 6 one can notice that the higher Ma produces the higher circulation either before the passage of the reflected shock (open tube condition) or after the re-shock process in all investigated cases. Also it is clear that the values of circulation after the re-shock process are higher than the circulation values before the re-shock. Therefore, it is obvious that the re-shock condition allows more instability and evolution of the interfaces and increases the vorticity generation, which produces high circulation enhancing the mixing process.

VII. CONCLUSIONS

The aim of this work was to study the physical behavior of heterogeneous bubbles which were subjected to high intensity shock waves under re-shock condition. Therefore, a numerical algorithm has been built to solve a compressible two component flow model. Three different air/gas configurations at atmospheric pressure that represent heavy/light, close molecular weight and light/heavy arrangements have been studied. The numerical results have been compared with available experimental data for shock-bubble interaction with open shock tube condition. These comparisons have shown that the numerical results are in a good agreement with the experimental data. Then the numerical simulations have been further extended to investigate the effect of the shock Mach number on the interface evolution and vorticity generation under re-shock condition. Thus, the effect of the shock velocity, molecular weight and density ratio on the interface evolution and the vortex formation have been shown and discussed for all investigated problems.

REFERENCES

[1] J. Yang, T. Kubota, and E. E. Zukoski, "*Applications of shock-induced mixing to supersonic combustion*," *AIAA Journal*, vol. 31, pp. 854-862 (1993).

[2] J. D. Lindl, R. L. McCrory, and E. M. Campbell, "*Progress toward ignition and burn propagation in inertial confinement fusion*," *Physics Today*, vol. 45, pp. 32-40 (1992)

[3] J. Haas, and B. Sturtevant, *"Interaction of weak shock waves with cylindrical and spherical gas inhomogeneities*," *Journal of Fluid Mechanics*, vol. 181, pp. 41-76 (1987).

[4] G. Layes, G. Jourdan, and L. Houas, "*Distortion of a spherical gaseous interface accelerated by a plane shock wave*," *Physical Review Letters*, vol. 91, 174502 (2003)

[5] G. Layes, and O. Le Métayer, "*Quantitative numerical and experimental studies of the shock accelerated heterogeneous bubbles motion,*" *Physics of Fluids*, vol. 19, 042105 (2007)

[6] G. Layes, G. Jourdan, and L. Houas, *"Experimental study on a plane shock wave accelerating a gas bubble*," *Physics of Fluids*, vol. 21, 074102 (2009)

[7] B. D. Collins, and J. W. Jacobs, "*PLIF flow visualization and measurements of the Richtmyer-Meshkov instability of an air/SF_6 interface," Journal of Fluid Mechanics*, vol. 464, pp. 113-136 (2002)

[8] D. Ranjan, J. Niederhaus, B. Motl, M. Anderson, J. Oakley, and R. Bonazza, *"Experimental investigation of primary and secondary features in high Mach number shock-bubble interaction*," *Physical Review Letters*, vol. 98, 024502 (2007)

[9] X. Luo, T. Si, J. Yang, and Z. Zhai, . "*A Cylindrical converging shock tube for shock interface studies*," *Review of Scientific Instruments*. vol. 85, 015107. (2014)

[10] J. J. Quirk, and S. Karni, "*On the dynamics of shock-bubble interaction*," *Journal of Fluid Mechanics*, vol. 318, pp. 129-163 (1996)

[11] J. Giordano, and Y. Burtschell, "*Richtmyer-Meshkov instability induced by shock-bubble interaction: Numerical and analytical studies with experimental validation*," *Physics of Fluids*, vol. 18, 036102 (2006)

[12] F. Diegelmann, S. Hickel, N. A. Adams *"Three-dimensional reacting shock–bubble interaction*" *Combustion and Flame*, vol. 181, pp. 300-314, (2017)

[13] J. Ding, T. Si, M. Chen, Z. Zhai, X. Lu and X. Luo *"On the interaction of a planar shock with a three-dimensional light gas cylinder*," *Journal of Fluid Mechanics*. Vol. 828, pp. 289–317, (2017)

[14] A. Bagadir, and D. Drikakis, *"Mach number effects on shock-bubble interaction," Shock Waves*, vol.11, pp. 209-218 (2001)

[15] J. H. J. Niederhaus, J. A. Greenough, J. G. Oakley, D.Ranjan, M. H. Anderson, and R. Bonazza, "*A computational parameter study for the three-dimensional shock-bubble interaction," Journal of Fluid Mechanics*, vol. 594, pp. 85-124 (2008)

[16] P. Georgievskiy, V. Levin and O. Sutyrin "Shock Focusing upon Interaction with Heavy Gas Bubble of Different Density*," J. Phys.: Conf. Ser*. 1141 012084 (2018)

[17] D. Ranjan, J. Oakley, and R. Bonazza, "*Shock-bubble interactions*," *Annual Review of Fluid Mechanics*, vol. 43, pp. 117-140 (2011)

[18] N. Haehn, C. Weber, J. Oakley, M. Anderson, D. Ranjan, and R. Bonazza, "*Experimental study of the shock–bubble interaction with reshock*," *Shock Waves*, vol. 22, pp. 47-56 (2012)

[19] C. Bailie, J. A. McFarland, J. A. Greenough, and D. Ranjan, "*Effect of incident shock wave strength on the decay of Richtmyer–Meshkov instability-introduced perturbations in the refracted shock wave," Shock Waves*, vol.22, pp. 511-519 (2012)

[20] Y. J. Zhu, G. Dong, B. C. Fan, and Y. X. Liu, *"Formation and evolution of vortex rings induced by interactions between shock waves and a low-density bubble*," *Shock Waves*, vol. 22, pp. 495-509 (2012)

[21] A. K. Kapila, R. Menikoff, J. B. Bdzil, S. F. Son, and D. S. Stewart, "*Two-phase modeling of deflagration to detonation transition in granular materials: Reduced equations*," *Physics of Fluids*, vol. 13, pp. 3002-3024 (2001)

[22] R. Saurel, F. Petitpas, and R. A. Berry, "*Simple and efficient relaxation methods for interfaces separating compressible fluids, cavitating flows and shocks in multiphase mixtures," Journal of Computational Physics*, vol. 228, pp. 1678–1712 (2009)

[23] G. Strang, "*On the construction and comparison of difference schemes. SIAM Journal on Numerical Analysis*, vol. 5, pp. 506-517 (1968)

[24] M. H. Lallemand, A. Chinnayya, and O. Le Métayer, "*Pressure relaxation procedures for multiphase compressible flows*," *International Journal for Numerical Methods in Fluids*, vol. 49, pp. 1-56 (2005)